Vortex-induced drag and the role of aspect ratio in undulatory swimmers

V. Raspa, S. Ramananarivo, B. Thiria, and R. Godoy-Diana

Citation: Physics of Fluids (1994-present) **26**, 041701 (2014); doi: 10.1063/1.4870254
View online: http://dx.doi.org/10.1063/1.4870254
View Table of Contents: http://scitation.aip.org/content/aip/journal/pof2/26/4?ver=pdfcov
Published by the AIP Publishing

PHYSICS OF FLUIDS **26**, 041701 (2014)

Vortex-induced drag and the role of aspect ratio in undulatory swimmers

V. Raspa, S. Ramananarivo, B. Thiria, and R. Godoy-Diana[a)]
Physique et Mécanique des Milieux Hetérogènes (PMMH UMR 7636), CNRS, ESPCI ParisTech, UPMC (Paris 6), Univ. Paris Diderot (Paris 7), 10 rue Vauquelin, 75231 Paris Cedex 5, France

(Received 6 January 2014; accepted 17 March 2014; published online 2 April 2014)

During cruising, the thrust produced by a self-propelled swimmer is balanced by a global drag force. For a given object shape, this drag can involve skin friction or form drag, both being well-documented mechanisms. However, for swimmers whose shape is changing in time, the question of drag is not yet clearly established. We address this problem by investigating experimentally the swimming dynamics of undulating thin flexible foils. Measurements of the propulsive performance together with full recording of the elastic wave kinematics are used to discuss the general problem of drag in undulatory swimming. We show that a major part of the total drag comes from the trailing longitudinal vortices that roll-up on the lateral edges of the foils. This result gives a comparative advantage to swimming foils of larger span thus bringing new insight to the role of aspect ratio for undulatory swimmers. © *2014 AIP Publishing LLC*. [http://dx.doi.org/10.1063/1.4870254]

Generation of propulsive forces by means of anguilliform kinematics is a feature shared in nature by a wide group of aquatic animals of very different characteristics.[1–3] Anguilliform-like swimmers achieve propulsion with high hydromechanical efficiency by propagating bending waves along the body, from head to tail.[4,5] The mechanisms of thrust production at play in this type of undulatory swimming have been extensively studied since the mid 1950s.[4,6–10] Depending on the Reynolds number, which measures the importance of viscous versus inertial effects, the fluid acts on the body either through local friction (resistive forces) or added mass effects (reactive forces). In both cases, the global thrust T is obtained by spatial integration of those local contributions, and is highly dependent on the kinematics of the undulating body.

The cruising regime of constant velocity U chosen by the swimmer is characterized by the balance between thrust and drag forces acting on the body. The quantification of the total drag with respect to the swimming parameters is a crucial point for the evaluation of the propulsive performance and efficiency, but the problem is non-trivial since the total drag involves various contributions (e.g., viscous friction or wake drag). Viscous friction has been more largely addressed in the fish-like swimming context. In particular, Lighthill[11] predicted that the "thinning" of the boundary layer caused by an undulatory motion would cause an increase of friction with respect to the flat-plate type skin friction. This early hypothesis has been recently quantified.[12] The problem of wake drag has been thoroughly studied in the case of bluff-body flows. Nevertheless, results are difficult to extrapolate to an object whose shape is changing with time. A description of the total drag is thus not straightforward for self-propelled anguilliform swimmers.

In this paper, we address experimentally the problem of drag by studying the performance of self-propelled swimming foils with different aspect ratios. The anguilliform kinematics is here reproduced by using the elastic response of a plate to a periodic actuation applied at one end; this simple implementation of an undulatory motion (relying on elasticity) has been recently proven to

[a)]Electronic mail: ramiro@pmmh.espci.fr

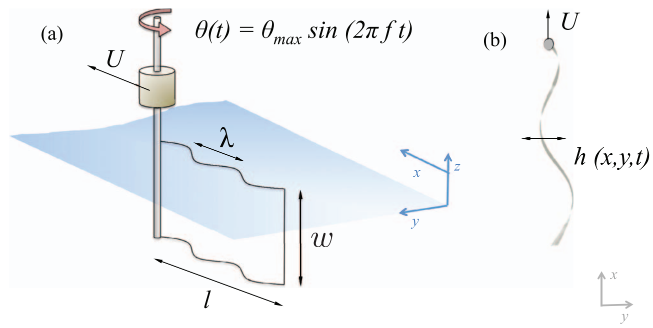

FIG. 1. Experimental setup. (a) Sketch of the mechanical swimmer submerged in the tank. Definition of driving parameters as well as swimmer's dimensions and velocity. (b) Camera view of the swimmer. The local body deflection $h(x, y, t)$ is also indicated.

be an effective manner of addressing fish-like swimming problems.[13–15] We quantify the role of the aspect ratio of the body in the performance of the swimmers, showing in particular that the drag experienced by the foils while swimming is mainly independent of the span. This finding allows us to pinpoint the main source of drag in the system and to discuss the role of aspect ratio on swimming efficiency, both being important issues for the future design of artificial fish-mimicking swimmers.

The experiment is performed in a free-surface water tank (0.9 m × 0.8 m × 0.5 m) where an artificial anguilliform-like swimmer is fully submerged and allowed to move freely in a rectilinear motion using an air bearing rail (see Figure 1). The body consists in a rectangular foil made of 130 μm thick Mylar whose bending rigidity is $B = 1.02 \times 10^{-3}$ N m. The foil is clamped to a cylindrical axis ($d = 0.005$ m in diameter) that constitutes the head of the swimmer and sets the swimming depth in the water bulk. A pitching motion is imposed that generates self-propulsion by creating a backward propagating undulation along the flexible body. The rotational oscillation of the head is controlled with 0.5° of precision by a small stepper and a sine wave driving curve of amplitude $\theta_{max} = 50°$ and frequency f ranging from 1 to 5 Hz. Swimmers of length $l = 0.15$ m and different spans w were tested, giving aspect ratios ($AR = w/l$) ranging from 0.1 to 0.7.

The swimming body kinematics is recovered from high speed camera recordings for each set of parameters. The local body deflection and the tail beating amplitude (A_r) are then extracted. Figure 2(a) (that corresponds to an $AR = 0.7$ foil driven at $f = 2.5$ Hz) exemplifies a typical amplitude envelope. The kinematic results, displayed in Fig. 2(b), show that A_r decreases with the driving frequency (due to an increased dissipation with f, see Ref. 15), but is not depending on the foil's aspect ratio. The forward motion of the foil along the swimming axis is also tracked, following the location of its head in time ($x(t)$). Figure 2(c) illustrates a run, showing that after a clear transitory the swimmer reaches constant velocity. The swimming velocity U is thus calculated from the slope of the final stretch of the corresponding $x(t)$ profile, where thrust and drag are on average balanced. Figure 3(a) shows U as a function of the driving frequency for all the experiments reported here. As expected, the swimming velocity is found to be an increasing function of the driving frequency. Additionally, under the same forcing, larger aspect ratios swim faster. The measured values of U give Reynolds numbers $Re_l = Ul/\nu$, with ν the kinematic viscosity of water, between 5000 and 18 000.

The propulsive force can be recovered from the displacement curve of the swimmer. As in Ref. 16, measurements are fitted with $x(t) = \frac{m}{\gamma} \log\left[\cosh \frac{\sqrt{\gamma F}}{m} t\right]$, solution of the $m\ddot{x} + \gamma \dot{x}^2 = F$ simplified dynamical model of the system. Where m is the total mass of the swimmer, $\gamma \dot{x}^2$ is a quadratic hydrodynamic drag term, and F is the propulsive force. Both γ and F are outputs of the nonlinear least-squares fitting procedure used to match the experimental $x(t)$ curve to the analytical solution of the dynamical equation.[17] Figures 3(b) and 3(c) present the results of thrust generation as a function of frequency and foil span, showing as expected that for a given driving frequency, foils with larger span produce higher thrust. In addition, Fig. 3(c) indicates that F is a linear function of the aspect ratio.

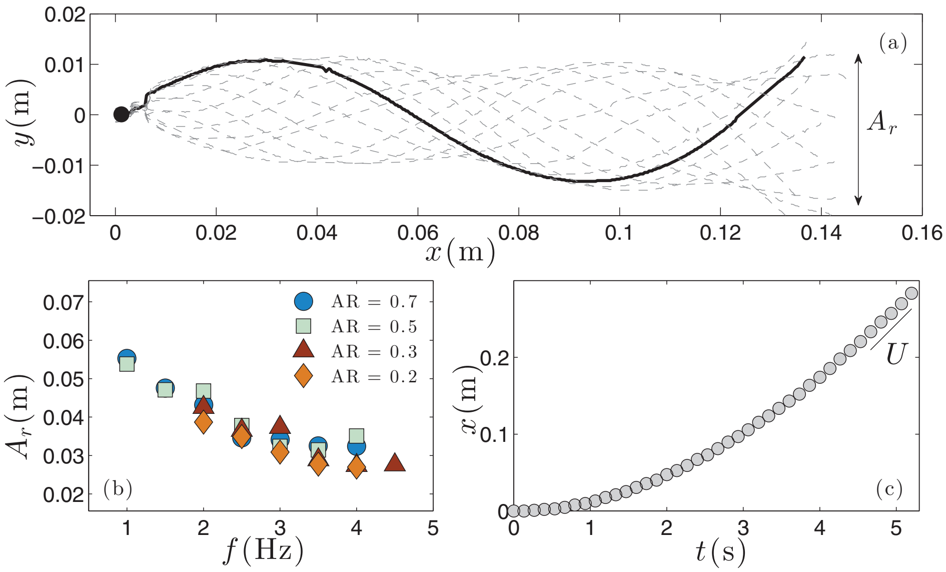

FIG. 2. Kinematics of the undulating foil. (a) Superposed envelopes from a typical video tracking. (b) Amplitude of the tail A_r as a function of the driving frequency for every swimmer. (c) Typical displacement curve $x(t)$, obtained from camera recording. The swimming velocity U is correspondingly calculated from $x(t)$. On the example, $AR = 0.7$ and $f = 2.5$ Hz.

Since the foil kinematics and the value of the resulting thrust are both measurable in this setup, the performance of the swimmer can be compared with Lighthill's elongated-body theory (EBT) predictions. This model provides an estimate of the mean thrust produced by a given kinematics $h(x, t)$, where h is the lateral deflection of the slender body with respect to the swimming axis. This propulsive force is shown to depend only on the motion of the tail $x = l$ (with l the length of the swimmer): $F = 1/2AM\left[\overline{(\partial h/\partial t)_l^2} - U^2\overline{(\partial h/\partial x)_l^2}\right]$. AM is the added mass of water that is accelerated by the body movements. As F and the derivatives of h are both available from the 2D-kinematics presented in Fig. 2,[18] AM can be estimated from the fitting of Lighthill's expression to the corresponding force data set for each aspect ratio (see Fig. 3(b)). The results are displayed in the inset in Fig. 3(c). The added mass is observed to depend linearly on the aspect ratio, meaning that all the swimmers push the same amount of fluid per unit span. This result is consistent with the fact that the measured force per unit span is a constant (knowing that the tail kinematics is independent of the swimmer span as shown in Fig. 2(b)).

For all the aspect ratios studied, the foil kinematics, added mass, and thrust per unit span are thus the same. However, foils with different aspect ratios do not reach the same velocities. This difference

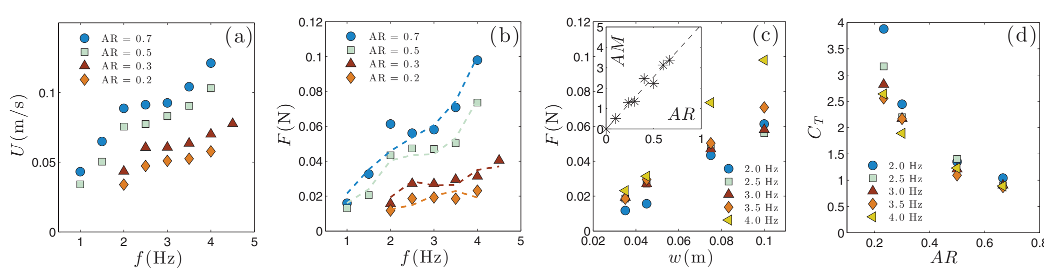

FIG. 3. (a) Self-propelled swimming velocity U as a function of the forcing frequency f for four aspect ratios. (b) and (c) Propulsive force F as a function of the forcing frequency and of the foil width, respectively. In (b) measurements are presented in symbols for different swimmers, together with the corresponding Lighthill's prediction (dashed lines). The inset in (c) shows the added mass coefficient AM as a function of the aspect ratio AR. (d) Dimensionless thrust coefficient as a function of the aspect ratio.

shows when calculating the standard non-dimensional net thrust coefficient $C_T = F/(\frac{1}{2}\rho U^2 wl)$, which is displayed in Fig. 3(d) as a function of the aspect ratio. The dimensionless representation shows here that C_T diminishes with increasing aspect ratio (because U is changing with AR). Larger aspect ratio foils also show less scatter in C_T over the frequency range explored.

Aspect ratio thus significantly influences the performance of the present undulatory swimmers. Given the w-dependencies described above, the hierarchy observed in the swimming speed as a function of span (Fig. 3(a)) can only be explained studying the way the hydrodynamic drag varies with AR. Considering the quadratic term used in the dynamic model that accurately describes the swimming position $x(t)$, one may write the general form $D = \frac{1}{2}\rho U^2 wlC_D$, with C_D a global drag coefficient. Evidently, because the same scaling is used to write thrust and drag in terms of dimensionless coefficients, the self-propelled cruising force balance can be rewritten as $C_T = C_D$. Two main approaches have been reported in the literature to express C_D for an undulating body. The first one considers skin friction as the main contribution to drag, either ignoring the undulation and considering the drag on a flat plate[13] or computing the increase in skin friction due to the thinning of the boundary layer.[5,12] As a first approximation, one can thus write for skin friction $C_{D\,\mathrm{skin}} = c_1 Re_l^{-1/2}$, with c_1 a constant of order unity. A more realistic skin friction coefficient should of course consider the 3D nature of the flow: it should take into account on the one hand the spanwise modulation that can be expected due to the finite size of the swimmer, and on the other the streamwise evolution of the boundary layer. These two effects, which will not be considered here, will have to be addressed in conjunction with Lighthill's boundary layer thinning due to wall-normal motion.[12] The other source of dissipation is a bluff-body type form drag, which is usually written from a quasi-two-dimensional (Q2D) perspective using the area swept by the trailing edge wA_r as reference surface.[15] This gives $C_{D\,\mathrm{form}} = c_2 A_r/l$, again, c_2 being a constant of order one (smaller than one for streamlined bodies). Examining the two previous expressions, it is clear that none of them, nor a combination $C_D = C_{D\,\mathrm{skin}} + C_{D\,\mathrm{form}}$ is capable of explaining the observed behaviour of C_T in Figure 3(d) as both are independent of the aspect ratio.

However, another source of inertial dissipation may occur. The Q2D form drag expression mentioned above is built from the observation of the typical reverse Bénard-von Kármán vortex structure observed in a stream-wise-cross-stream (xy) midplane section of the wake, assuming that this structure is a section of what happens all along the span of the swimmer. For three-dimensional geometries, this is nonetheless only part of a complex vortex system and each vortex in the xy plane continues over two branches shed by the top and bottom edges of the swimmer[19,20] that constitute a pair of longitudinal vortices. These structures are known as trailing vortices in the context of wing theory[21] and have been shown to account for a substantial part of the drag in bluff-body problems[22] (the so-called *induced drag*). Figure 4 shows a visualization of a yz cross section perpendicular to the swimming direction. Indeed, two pairs of counter-rotating vortices can be observed, which constitute the longitudinal structures that will be periodically shed in the wake. It is worth noticing that the typical size of the vortex cores does not seem to be affected by the size of the swimmer. This can be understood by the fact that the characteristic shear layer length feeding the longitudinal vortex scales only with the transversal velocity at the edge and is independent of the span. This mechanism is then a constant contribution to the total drag for all the swimmers tested. Quantitatively, longitudinal vortices induce drag through the depression in each vortex core, which can be related to their rotational kinetic energy in terms of the circulation Γ of each vortex. To estimate the order of magnitude of the average contribution to the total drag of a pair of vortices such as those illustrated in Fig. 4, we follow the idea proposed in Ref. 23 and model the vorticity field in the yz-plane as a pair of counter-rotating Rankine vortices of circulation Γ. This leads to the expression $D_v \approx 3\rho\Gamma^2/8\pi$ for the vortex drag (see the paragraph of Vortex-Induced Drag Model), which is a span-independent contribution. We have compared the values of $C_{D\,\mathrm{vortex}}$ obtained from this calculation to the drag coefficients of skin friction and quasi-2D form drag (see Figure 5(a)). For the comparison we have fixed the numerical constants of order unity to $c_2 = c_3 = 1$, corresponding to form and vortex drag, and $c_1 = 2.66$, the standard value for flat plate skin friction. The circulation Γ needed to calculate vortex drag has been estimated for all the experimental points in terms of the kinematics of the trailing edge considering that the shear layer produced by the moving tip of the foil feeds a vortex during each half period. Writing $u = A_r f$ as the order of magnitude of the tip velocity,

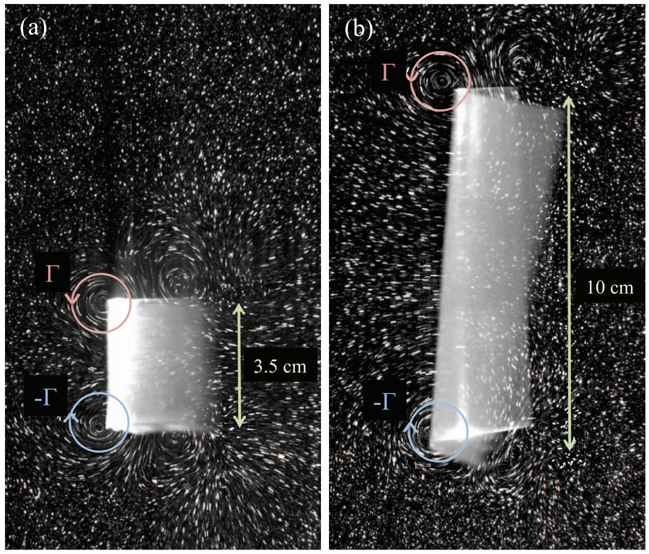

FIG. 4. Visualisation of the longitudinal vortical structures on top and bottom edges of the foils. The driving frequency was set to 1 Hz. (a) $AR = 0.2$. (Multimedia view) [URL: http://dx.doi.org/10.1063/1.4870254.1]. (b) $AR = 0.7$. (Multimedia view) [URL: http://dx.doi.org/10.1063/1.4870254.2]. Particle streaks are illuminated by a vertical laser sheet placed at the foils' mid length plane.

an estimate of the circulation can be written as $\oint u dl$ over a circular path of length πA_r, which gives $\Gamma \approx \pi A_r^2 f$. This yields $C_{D\,\mathrm{vortex}} \approx \frac{3}{2}\pi f^2 A_r^4/U^2 l w\, c_3$. Additionally, for one data point for each foil, particle image velocimetry (PIV) measurements performed on the yz-plane images of Fig. 4 have been used to obtain a direct measurement of the maximum circulation of these longitudinal vortices. The circulation at each time frame is calculated using an integration of the velocity field obtained by PIV over a square contour centered at the position of the extrema of vorticity (as in Ref. 24). The size of the contour was fixed as two times the characteristic size of a Gaussian fit of the most intense vorticity patch recorded during one cycle, a value large enough to obtain convergence of the calculated circulation when increasing the contour size. The obtained values of $C_{D\,\mathrm{vortex}}$ are shown in Figure 5(a) together with $C_{D\,\mathrm{skin}}$ and $C_{D\,\mathrm{form}}$. It appears clearly that $C_{D\,\mathrm{vortex}}$ represents the main source of drag. Although to consider an "average" longitudinal vortex shed at each edge of the foil might be a strong simplification of this complex system, it certainly allows us to show that vortex-induced drag is the only term that can balance the observed thrust coefficients in terms of order of magnitude.

Thus, for real swimmers of finite size, the main source of dissipation is independent of the span, an observation that cannot be accounted for with the usual models based on skin friction, which

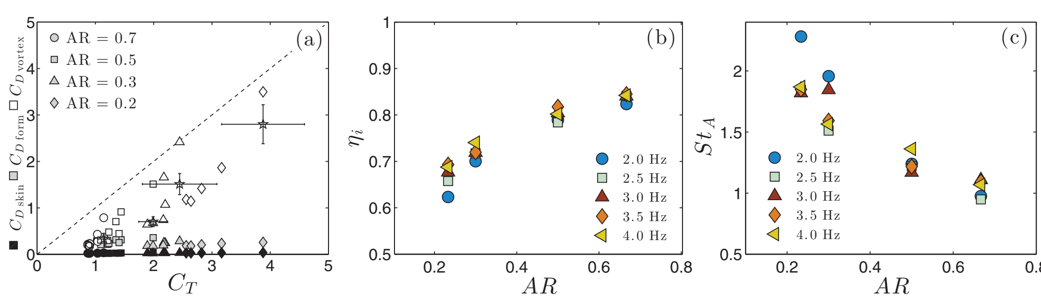

FIG. 5. (a) Drag coefficients $C_{D\,\mathrm{skin}}$, $C_{D\,\mathrm{form}}$, and $C_{D\,\mathrm{vortex}}$ compared to C_T. The dashed line represents the balance of drag and thrust. The stars are the values of $C_{D\,\mathrm{vortex}}$ obtained using a circulation calculation from PIV measurements on the yz-plane images of Fig. 4 for $f = 1$ Hz. (b) Ideal efficiency η_i and (c) Strouhal number St_A as a function of the aspect ratio.

inherently give drag per-unit-span. Drag being mostly given by a mechanism independent of the foil span determines as a direct consequence a comparative advantage to large aspect ratio foils. The physical mechanism behind this observation can be readily understood by observing that while the thrust force increases when the span of the foil increases, the stream-wise vortices produced at the top and bottom edges of the foil remain relatively unchanged when increasing the span, so that vortex-induced drag represents a larger penalty for the smaller foils. This can be seen using the C_T values to compute an ideal efficiency, which we write, following Ref. 25, as $\eta_i = 2/(1 + (1 + C_T)^{1/2})$. A decreasing thrust coefficient thus results in an increasing efficiency as shown in Fig. 5(b), a trend correlated also with a decreasing value of the Strouhal number St_A commonly used to describe flapping-based propulsion (Fig. 5(c), see also Ref. 15). In conclusion, although a standard 2D Lighthill-theory analysis is reasonable for the prediction of the thrust of such swimmers, drag, though, needs to consider the flow as a full 3D structure. The analysis of the present paper can be useful to improve our quantitative knowledge about drag in undulatory propulsion, which is a fundamental issue for understanding the energy budget in any autonomous swimmer.

Vortex-Induced Drag Model: We recall here the main points of Beaudoin's derivation[23] of the formula for the vortex drag model D_v used above, which considers a pair of counter-rotating Rankine vortices. Each vortex is defined as: $u_\theta(r < R) = \frac{\Gamma r}{2\pi R^2}$ and $u_\theta(r > R) = \frac{\Gamma}{2\pi r}$, where R is the vortex radius and Γ its circulation. The pressure in each vortex core can be obtained writing the balance of the radial pressure gradient and the centrifugal force

$$\frac{dp}{dr} = \frac{\rho\Gamma^2}{4\pi^2 R^4} r.$$

Writing p_0 for the pressure when $r \to \infty$ leads to the expression for the pressure field:

$$p(r < R) = p_0 - \frac{\rho\Gamma^2}{8\pi^2 R^2}\left[2 - \left(\frac{r}{R}\right)^2\right], \quad p(r > R) = p_0 - \frac{\rho\Gamma^2}{8\pi^2 R^2}\frac{R^2}{r^2}.$$

Now, considering two vortices separated by a distance d in the yz plane (transverse to the swimming direction in the context of the present paper), and assuming that the pressure in each vortex core is not significantly affected by the presence of the other (which is reasonable because $d > 2R$ and $p(r > R)$ decays rapidly), we can keep only the pressure field in the core $p(r < R)$ to estimate the vortex drag. The corresponding pressure term in the drag equation obtained applying the conservation of momentum to a finite volume containing the swimmer (bounded by equal upstream and downstream surfaces Σ_S) reads (see also Refs. 22 and 26):

$$\int_{\Sigma_s} (p_0 - p)d\sigma = 2\int_{\Sigma_s} \frac{\rho\Gamma^2}{8\pi^2 R^2}\left[2 - \left(\frac{r}{R}\right)^2\right] = \frac{3\rho\Gamma^2}{8\pi},$$

where the actual surface of integration Σ_S is the area of the two vortex cores.

We gratefully acknowledge support by EADS Foundation through project "Fluids and elasticity in biomimetic propulsion."

[1] P. W. Webb, "Body Form, Locomotion and foraging in aquatic vertebrates," Am. Zool. **24**, 107–120 (1984).
[2] G. B. Gillis, "Undulatory locomotion in elongate aquatic vertebrates: Anguilliform swimming since Sir James Gray," Am. Zool. **36**, 656–665 (1996).
[3] R. W. Blake, "Fish functional design and swimming performance," J. Fish Biol. **65**, 1193–1222 (2004).
[4] M. J. Lighthill, "Note on the swimming of slender fish," J. Fluid Mech. **9**, 305–317 (1960).
[5] M. J. Lighthill, "Aquatic animal propulsion of high hydromechanical efficiency," J. Fluid Mech. **44**, 265–301 (1970).
[6] G. I. Taylor, "Analysis of the swimming of long and narrow animals," Proc. R. Soc. London, Ser. A **214**, 158–183 (1952).
[7] K. E. Machin, "Wave propagation along flagella," J. Exp. Biol. **35**, 796–806 (1958).
[8] T. Y. Wu, "Hydromechanics of swimming propulsion. Part 1. Swimming of a two-dimensional flexible plate at variable forward speeds in an inviscid fluid," J. Fluid Mech. **46**, 337–355 (1971).
[9] C. Eloy and L. Schouveiler, "Optimisation of two-dimensional undulatory swimming at high Reynolds number," Int. J. Nonlinear Mech. **46**, 568–576 (2011).
[10] F. Candelier, F. Boyer, and A. Leroyer, "Three-dimensional extension of Lighthill's large-amplitude elongated-body theory of fish locomotion," J. Fluid Mech. **674**, 196–226 (2011).
[11] M. Lighthill, "Large-amplitude elongated-body theory of fish locomotion," Proc. R. Soc. London, Ser. B **179**, 125–138 (1971).

[12] U. Ehrenstein and C. Eloy, "Skin friction on a moving wall and its implications for swimming animals," J. Fluid Mech. **718**, 321–346 (2013).
[13] S. Alben, C. Witt, T. V. Baker, E. Anderson, and G. V. Lauder, "Dynamics of freely swimming flexible foils," Phys. Fluids **24**, 051901 (2012).
[14] P. A. Dewey, B. M. Boschitsch, K. W. Moored, H. A. Stone, and A. J. Smits, "Scaling laws for the thrust production of flexible pitching panels," J. Fluid Mech. **732**, 29–46 (2013).
[15] S. Ramananarivo, R. Godoy-Diana, and B. Thiria, "Passive elastic mechanism to mimic fish-muscles action in anguilliform swimming," J. R. Soc. Interface **10**, 20130667 (2013).
[16] V. Raspa, R. Godoy-Diana, and B. Thiria, "Topology-induced effect in biomimetic propulsive wakes," J. Fluid Mech. **729**, 377–387 (2013).
[17] A Monte Carlo scheme was used to estimate the error in the force measurement: Displacement measurements were randomly and independently perturbed with their range of variability to propagate that uncertainty to the force measurement through the nonlinear fitting. The resulting error is always smaller than the marker size in Figure 3.
[18] The derivatives of h are evaluated as a standard discrete approximation to differentiation. A spline is fitted to the kinematics measurements prior to differentiation. The relative error on the time derivatives is $\approx$3%. For the spatial derivative, a linear fit of the last portion (1/5) of the foil is first performed, whose slope gives $\partial h/\partial x$. The uncertainty in this case is related to the goodness of this fit, which has a correlation coefficient of 0.94. The main source of uncertainty in the calculation of Lighthill's force estimate, however, arises when averaging the square of the time and space derivatives over a period, because some parts of the cycle are missing owing to defects in the video tracking. The overall average error in the force estimate is of approximately 8%.
[19] J. H. J. Buchholz and A. J. Smits, "The wake structure and thrust performance of a rigid low-aspect-ratio pitching panel," J. Fluid Mech. **603**, 331–365 (2008).
[20] A. P. S. Bhalla, B. E. Griffith, and N. A. Patankar, "A forced damped oscillation framework for undulatory swimming provides new insights into how propulsion arises in active and passive swimming," PLoS Comput. Biol. **9**, e1003097 (2013).
[21] G. K. Batchelor, "Axial flow in trailing line vortices," J. Fluid Mech. **20**, 645–658 (1964).
[22] J. L. Aider, J. F. Beaudoin, and J. E. Wesfreid, "Drag and lift reduction of a 3D bluff-body using active vortex generators," Exp. Fluids **48**, 771–789 (2009).
[23] J. F. Beaudoin, "Contrôle actif d'écoulement en aérodynamique automobile," Ph.D. thesis (École des Mines de Paris, 2004).
[24] R. Godoy-Diana, C. Marais, J. L. Aider, and J. E. Wesfreid, "A model for the symmetry breaking of the reverse Bénard-von Kármán vortex street produced by a flapping foil," J. Fluid Mech. **622**, 23–32 (2009).
[25] J. M. Anderson, K. Streitlien, D. S. Barret, and M. S. Triantafyllou, "Oscillating foils of high propulsive efficiency," J. Fluid Mech. **360**, 41–72 (1998).
[26] P. Ardonceau and G. Amani, "Remarks on the relation between lift induced drag and vortex drag," Eur. J. Mech. B Fluids **11**, 455–460 (1992).